Heliyon 9 (2023) e21039

Contents lists available at ScienceDirect

Heliyon

journal homepage: www.cell.com/heliyon

Effect of thiophene rings rigidity on dye-sensitized solar cell performance. Dithienothiophene versus terthiophene as $\pi-$ donor moiety

Samir Al-Taweel [a,*], Salah Al-Trawneh [a], Hmoud Al-Dmour [b], Osamah Al-Gzawat [a], Wasim Alhalasah [c], Marwan Mousa [b]

[a] Department of Chemistry, Faculty of Science, Mutah University, Mu'tah, 61710, Jordan
[b] Department of Physics, Faculty of Science, Mutah University, Mu'tah, 61710, Jordan
[c] Scientific Research and Innovation Support Fund, Ministry of Higher Education and Scientific Research, Amman, Jordan

ARTICLE INFO

Keywords:
Dye-sensitizer
Solar cells
Thin films
Molecular orbital
Energy levels

ABSTRACT

Solar cells are fabricated based on two new dyes. Dye acts as an additive to thin layer interface. The effect of the π-conjugated rigidity of the thiophene rings on the photovoltaic characteristics has been investigated. The structures of the dye 1 was based on dithieno [3,2-*b*:2′,3′-*d*] thiophene-2-cyanoacrylic acid, while dye 2 was based on [2,2':5′,2″-terthiophene]-5-cyanoacrylic acid and were confirmed by elemental analysis, mass spectrometry, ^{1}H NMR and ^{13}C NMR spectral data. The P3HT/dye 1/nc-TiO_2 solar cell produced the highest efficiency of 0.3 % with an open circuit voltage of 0.7 V compared to dye 2 solar cell. This has been attributed to the difference in energy levels of the dyes and location of their HOMO relative to conduction and valence bands of nc-TiO_2. The dye 1 has rigid fused thiophene rings and its HOMO is located between valence band of TiO_2 and HOMO of P3HT which leads to improve the charge carrier separation and increase the current density to reach 1.2 mA/cm^2.

1. Introduction

Hybrid photovoltaics cells, which are based on the junction between semiconducting material and organic dyes, so-called dye-sensitized solar cells (DSSCs), have attracted great interest in recent times. DSSCs have the potential of low-cost fabrication and ease of production, which makes them a good candidate for commercialization [1–4]. Race for solar cell commercialization continued, recently multifunctional composite photoanode containing TiO_2 hollow spheres (TiO_2-HSs), Au nanoparticles (AuNPs) and novel $NaYF_4$: Yb, Er@$NaLuF_4$: Eu@SiO_2 solar cells have been fabricated, reaching power conversion efficiency of 14.13 % using N719 dye [2b]. Also, addition of a nonpolar coadsorbants like chenooxycholic acid resulted in a remarkable increase in the open-circuit voltage as well as increase in PCE to 24.15 %[2c].

DSSCs contain five layers, a photo-anode composed of transparent conducting oxide substrate, semiconductor metal oxide film, a dye-sensitizer, redox couples/a hole transport material, and a counter electrode. Dye-sensitizer is an integral component responsible for the good performance of DSSCs, which plays a main role in light-gathering and electron excitation into semiconductors [4,5]. Organic sensitizers have a great advantage over noble Ru-complexes sensitizers, owing to their low cost, great variation in molecular

* Corresponding author.
E-mail address: s_altaweel@mutah.edu.jo (S. Al-Taweel).

https://doi.org/10.1016/j.heliyon.2023.e21039
Received 28 May 2023; Received in revised form 10 October 2023; Accepted 13 October 2023
Available online 17 October 2023

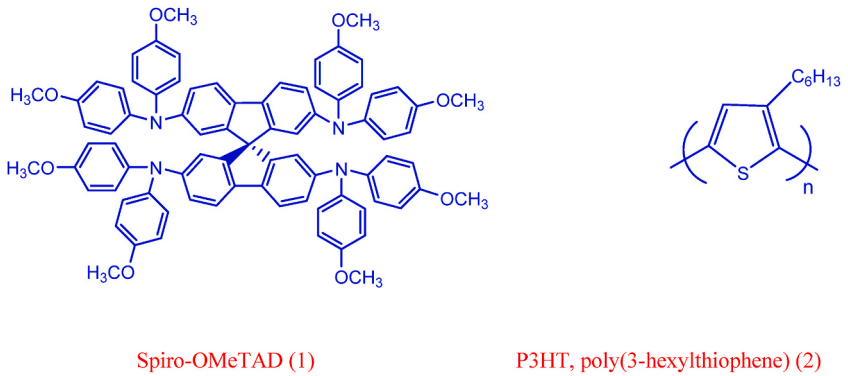

Fig. 1. Chemicals structure of Spiro-OMeTAD (1) and P3HT (2).

structures in addition to having high extinction coefficients [6,7]. Nevertheless, despite these attractions, the performance of DSSCs based on organic dyes has lagged behind those using metal-organic dyes, due to their high recombination losses and lower open-circuit voltage(V_{oc}) [8,9]. The hole transport material plays a critical role in DSSCs performance. It is deposited between the semiconductor layer and the metal contact, to prevent direct contact, and to minimize charge recombination [10,11]. One of the main challenges of DSSCs is the instability of HTM to thermal and environmental factors. One approach to minimize these factors is to design materials with low affinity for water. One of the most efficient and widely used hole transport material is spiro-OMeTAD (**1**), which is a twisted spirofluorene-based bulky molecule [11]. The chemical structure is shown in Fig. 1. P3HT, poly (3-hexylthiophene) (2) employed in conjunction with $MAPbBr_3$ perovskite solar cell show improved photo conversion efficiency (PCE) value up to 13 %, demonstrating the effectiveness of P3HT. Moreover, ideal HTM must fulfill several requirements. First, HOMO energy level of HTM should lie above the valence band energy of the semiconductor. Lowering the energy level of HOMO of the HTM towards the semiconductor energy level will result in higher open-circuit voltage (V_{os}) of DSSCs. Second, the hole-mobility should be greater than $10^{-3}cm^2V–^1S^{-1}$. Finally, suitable solubility in organic solvents to control the thickness of the HTM layer, which leads to lowering the resistance, which directly enhances cell fill factor (FF).

Ideal dye-sensitizer must fulfill the following criteria, the absorption spectrum should cover the Vis-NIR region, its extinction coefficient(Є) must be high to affect excellent light-harvesting. For excellent electron injection to the semiconductor, the LUMO of the dye should be localized near the anchoring group, usually carboxylic acid group, and above the conduction band of the semiconductor. The energy level of the HOMO for the dye should be lower than the energy level of the HTM to allow excellent regeneration of the dye. The periphery of the dye should be non-polar to minimize the direct contact to the anode and the dye should not cluster on the surface to avoid the lose of the excited state to the ground state. The well known type of organic dyes contains donor-to-acceptor (D-π-A) functionalities bridged by π-conjugated systems, such as oligothiophenes, thienothiophenes, dithienothiophenes, triphenylamine-derived porphyrin derivatives and carbazole donor moiety with thiophene as π-space and various anchoring acceptor moieties [12], where A is an electrophilic/acceptor group connected to the π-conjugated system such as cyanoacrylic acid or rhodanine-3-acetic acid. Dye-sensitizers containing thiophene based π–conjugated systems show an excellent combination of good electron transfer, reasonable band gap, lengthy molecular conjugation and chemical stability. In particular, with structural ring planarity, fused thiophenes have emerged as a novel class of $\pi-$ conjugated functionalities, notably, dithienothiophene and benzothienobenzothiophene [12,13]. Thus inspired, we investigated the effect of the π-conjugated rigidity of the thiophene rings on the photovoltaic characteristics.

In this work, dithieno[3,2-*b*:2′,3′-*d*]thiophene-2-cyanoacrylic acid(dye1) and [2,2':5,2″-terthiophene]-5-cyanoacrylic acid (dye 2) were prepared and characterized, then employed as sensitizers to investigate DSSC characteristics using poly(3-hexylthiophene) as a hole transport material(HTM).

2. Experimental details

2.1. General

N-butyllithium, N-formylpiperidine, lithium hydroxide, palladium(II) acetate, cesium fluoride were purchased from Aldrich. Thiophene was purchased from Janssen. 2-Mercaptoethyl acetate, calcium carbonate, potassium carbonate, sodium sulfate, dimethylformamide, tetrahydrofuran, magnesium sulfate and sodium hydroxide were purchased from across. Bromine, cuprous iodide, and phosphorus oxychloride were purchased from fluka.

THF was dried over benzophenone-ketyl radical and distilled under inert atmosphere, dichloromethane was dried over P_2O_5. Melting points were determined on a scientific melting point apparatus. ^1H NMR and ^{13}C NMR spectra were measured on a Bruker 400 MHz spectrometer with TMS as the internal standard in $CDCl_3$. HRMS were measured by ESI technique on Bruker APEx-IV instrument. CHN analysis was performed at University of Jordan. 2,2':5,2″-Terthiophene [14], 5-formyl-[2,2':5′,2":5"]terthiophene [15,16] and dithieno[3,2-*b*:2′,3′-*d*] thiophene [16,17] were prepared according to the respective literature procedures. Current–voltage (I–V)

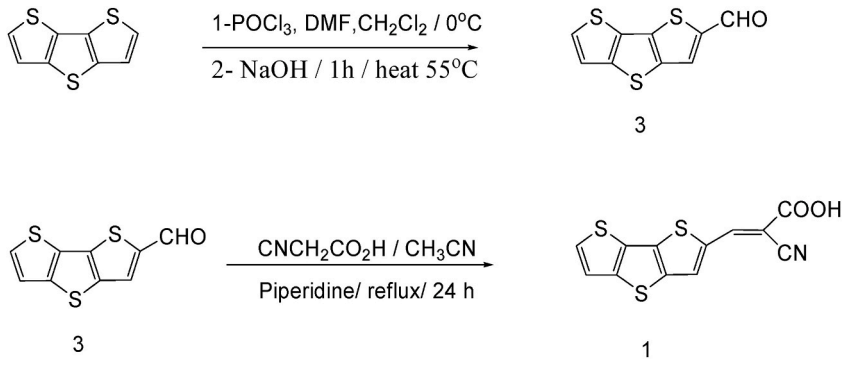

Scheme (1). Preparation of dithieno[3,2-*b*:2′,3′-*d*]thiophene-2-cyanoacrylic acid (1).

characteristics were measured using Keithley 237. The gold source was a 10 cm in length of wire cleaned by rubbing with Decon 90 and rinsed in hot ultrapure water. After drying in a stream of warm air, it was placed inside a tungsten boat in an Edwards AUTO 306 Turbo Evaporation System. A shadow mask was placed on the substrate which was then put in the Edwards system above the tungsten boat. After pumping to $\sim 10^{-5}$ torr, a gold film, 50 nm thick, was deposited through the shadow mask to form circular electrodes of ~3 mm in area. UV–Vis measurements were performed using Shimadzu 3150.

2.2. Preparation of dithieno[3,2-b:2′,3′-d] thiophene-2-cyanoacrylic acid (1)

Acetonitrile(5 ml) solution of dithieno[3,2-*b*:2'.3′-*d*]thiophene-2-carbaldehyde(3)(0.06 g, 0.267 mmol), cyanoacetic acid (0.066 g,0.78 mmol), and piperidine(0.1 g) was refluxed for 16 h under nitrogen atmosphere. The reaction mixture was added to hexane (15 ml) and HCl (15 ml,0.1 M. The orange to dark red precipitate was formed, this solid was filtrated to yield (0.067 g, 87 %) with m.p = 235 °C. ^{1}H NMR(DMSO-d_6, 400 MHz), ppm: $\delta = 8.57$ (s, 1H), 8.38 (s, 1H), 7.95 (d, 1H, $J = 5.2$ Hz), 7.63 (d, 1H, $J = 5.2$ Hz). ^{13}C NMR (100 MHz, DMSO-d_6): $\delta = 163.53, 147.32, 146.43, 141.49, 137.18, 135.83, 133.59, 132.05, 129.95, 121.80, 116.56, 97.97$. HRMS (EI): Calcd. For $C_{12}H_5NO_2S_3[M+Na]^+ = 313.93746$, found = 313.93795. Elemental analysis. Calcd. for $C_{12}H_5NO_2S_3$: C, 49.47; H, 1.73; N, 4.81. Found: C, 50,639; H, 2.889; N, 5.399. UV–Vis/emission was recorded in DMF, it shows λ_{max} at 374 nm with $\epsilon = 72000$ $M^{-1}cm^{-1}$, shows a weak broad emission at 500 nm with $\epsilon = 800$ $M^{-1}cm^{-1}$.

2.3. Preparation of dithieno[3,2-b:2'.3′-d]-2-carbaldehyde(3)

POCl3 (1 mmol, 0.153 g) was gradually added with stirring to a capped erlenmeyer flask containing DMF (1 mmol, 0.073 g) and dry CH_2Cl_2 (5 ml) at 0 °C. The mixture was then taken out of the ice bath and heated to approximately 40 °C until a clear pale yellow solution formed. In another flask containing a solution of dithieno[3,2-b:2'.3′-d] thiophene (0.15 g, 0.76 mmol) in 5 ml of dry CH_2Cl_2 at 0 °C, the Vilsmeier reagent was added drop by drop. The color of the mixture changed from yellow to red, and small crystals began to precipitate. After allowing it to stand at room temperature for 24 h, the CH_2Cl_2 was evaporated. Cold aqueous NaOH (1 M) was added to the residue, and the mixture was heated on a steam bath for 2 h. The resulting mixture was filtered, washed with water, and dried to yield a yellow powder. To obtain a yellow solid, column chromatography (hexane/CH2Cl2) was performed, resulting in 0.14 g with a melting point of 153 °C (yielding approximately 82 %). The ^{1}H NMR (DMSO-d_6, 400 MHz) spectrum showed peaks at $\delta = 9.99$ (singlet, 1H), 8.49 (singlet, 1H), 7.95 (doublet, 1H, $J = 5.2$ Hz), and 7.64 (doublet, 1H, $J = 5.2$ Hz). The ^{13}C NMR (DMSO-d_6, 100 MHz) spectrum displayed peaks at $\delta = 184.59, 146.31, 143.08, 141.48, 136.37, 132.75, 131.53, 129.93$, and 121.81.

2.4. Preparation of [2,2':5′,2″-terthiophene] 5-cyanoacrylic acid (2)

Acetonitrile(5 ml) solution with 5-formyl[2,2':5',2"] terthiophene(4)(120 mg, 0.43mmole), cyano acetic acid(80 mg, 0.86mmole) and piperidine (0.1 g) was refluxed for 24 h under a nitrogen atmosphere. The reaction mixture was added to petroleum ether (15 ml) and HCl (15 ml, 0.1 M). A dark red precipitate formed that was filtered to yield 110 mg, 80 % with m.p = 255 °C. ^{1}H NMR(DMSO-d_6, 400 MHz), ppm: $\delta = 8.84$ (s,1H), 7.98 (d, 1H, $J = 4$ Hz), 7.60 (m, 3H), 7.45 (d, 2H, $J = 4$ Hz), 7.39 (d, 1H, $J = 4$ Hz), and 7.13 (dd, 1H, $J = 4$ Hz).^{13}C NMR(DMSO-d_6/100 MHz), ppm: $\delta = 165.65, 163.55, 145.98, 144.88, 141.30, 138.35, 135.44, 134.06, 133.43, 128.64, 128.07, 126.66, 125.49, 125.21, 125.05$, and 116.67. UV-VS ($\lambda = 440$ nm, $CHCl_3$).

2.5. Synthesis

Dithieno[3,2-*b*:2′,3′-*d*]thiophene-2-cyanoacrylic acid(1) was prepared by a reaction of 2-formyldithieno[3,2-*b*:2′,3′-*d*]thiophene (3) with cyano acetic acid in acetonitrile using piperidine as base to afford dark red solid in 87 % yield, with m.p = 233–235 °C, as shown in Scheme (1).

2-Formyldithieno[3,2-*b*:2′,3′-*d*]thiophene(3) was prepared according to Vilsmeier method [17] by reacting dithieno[3,2-*b*:2′,3′-*d*]

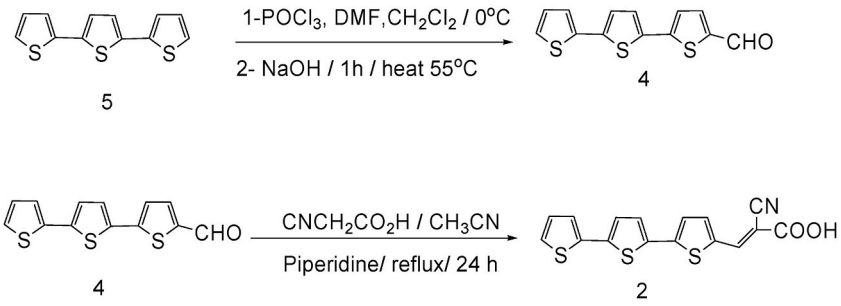

Scheme 2. Preparation of [2, 2': 5, 2″-terthiophene]-5-cyano acrylic acid (2).

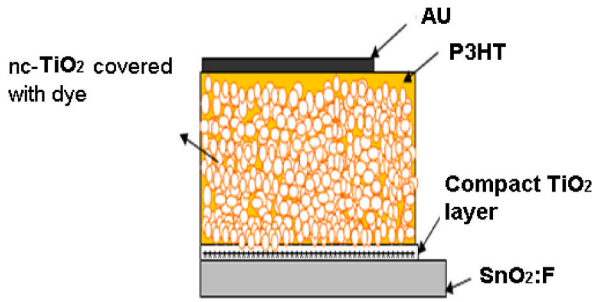

Fig. 2. Schematic diagrams of Au/P3HT/dye/nc-TiO_2/compact TiO_2/SnO_2:F solar cells.

thiophene with $POCl_3$ and DMF in CH_2Cl_2 at R.T, 2-formyldithieno[3,2-*b*:2′,3′-*d*] thiophene was isolated in 82 % as yellow solid with m. p = 154–155 °C. Starting with tetrabromothiophene as starting material, dithieno[3,2-*b*:2′,3′-*d*]thiophene was prepared via lengthy multistep method in subgram quantities, according to the literature procedure [16].

[2, 2':5, 2"]-Terthiophene-5-cyano acrylic acid (2) was prepared by a reaction of 5-formyl[2, 2': 5′, 2"]terthiophene(4) with cyano acetic acid in acetonitrile using piperidine as base to afford dark red solid in 87 % (Scheme 2). 5-Formyl- 2, 2': 5′, 2″-terthiophene (4) was prepared using Vilsmeier method, by reacting 2, 2': 5′, 2″-terthiophene (5) with $POCl_3$/DMF in CH_2Cl_2 at R.T in 78 % as yellow solid with m.p = 137 °C. 2, 2': 5′, 2″-Terthiophene(5) was prepared according the literature procedure [17].

2.6. Molecular orbital calculations

To gain a detailed understanding of the molecular structure and electron distribution of the organic dyes, their geometries were optimized using Density Functional Theory (DFT) calculations. The B3LYP functional with a 6-31G(d) basis set, a three-parameter compound functional developed by Becke, was employed for the geometry optimization and the determination of HOMO and LUMO energies [18–21]. All calculations were conducted using Gaussian-09 W software [21]. The calculated band gaps (E_{gap}) for dye 1 and dye 2 were found to be 2.189 eV (HOMO = 5.118 eV, LUMO = 2.929 eV) and 3.180 eV (HOMO = 6.203 eV, LUMO = 3.023 eV), respectively. These results suggest that dye 1 exhibits a higher degree of extended molecular conjugation and planarity in its fused thiophene rings compared to dye 2. The electron distribution of the HOMO is delocalized over the π system, with the highest electron density centered at the sulfur atom. On the other hand, the LUMO is located in the anchoring carboxylic group of cyanoacrylic acid.

2.7. Fabrication of the dye-sensitized solar cells

In this study, heterojunctions solar cells were fabricated using nanocrystalline *titanium dioxide layer coated by dye and* P3HT sandwiched between the two electrodes (Fig. 2). The bottom electrode is composed of a pre-cleaned fluorine-doped conducting tin oxide (FTO) glass plate coated with 20 nm of compact TiO_2 (sheet glass, 8 Ω/sq, 64 Solaronix). Doctor Blade techniques were used to spread nc-TiO_2 films on the bottom electrode. This film was sintered according to the reported procedure [22]. During sintering, the nc-TiO_2 films were burned to make electrical contact between their particles (at sintering temperature 220 °C–380 °C). The final film was transparent of light when the temperature reached 450 °C. This later process takes 130 min to assure producing anatase *TiO2* nanoparticles. The preparation of the dye/nc-TiO2/SnO2: F film involved several steps. Initially, SnO_2: F/nc-TiO_2 electrodes were immersed in a dye ethanol solution at room temperature for 12 h to allow the dye to be absorbed. In the subsequent step, the substrate was removed, rinsed with ethanol, and then dried under a nitrogen flow for 3 min. To prepare a solution of the p-type organic semiconductor P3HT in chloroform, a concentration of 15 mg/ml was achieved at a temperature range of approximately 45–61° Celsius to facilitate faster dissolution. A small amount of this solution was applied to the surface of the dye/nc-TiO_2/SnO_2: F film and left for a few seconds before being spun at 1000 rpm. The top electrode, composed of gold, was deposited onto the P3HT layer using an

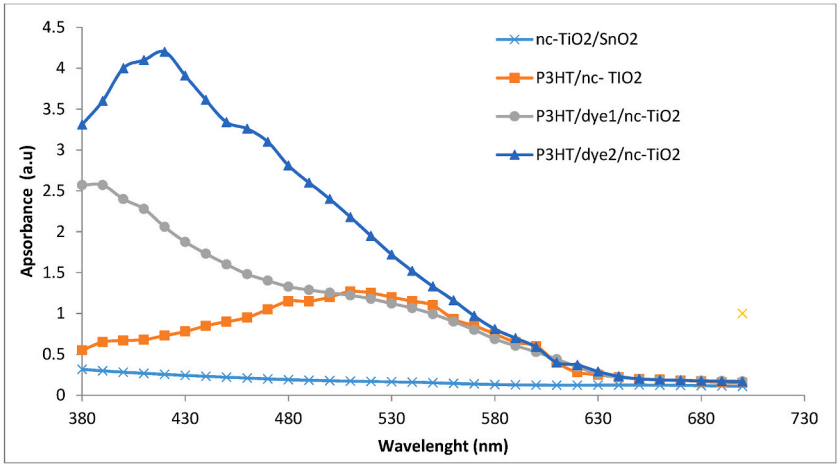

Fig. 3. UV-VS absorption spectra of the nc-TiO_2/SnO_2:Fn, nc-TiO_2/P3HT, nc-TiO_2/dye1/P3HT and nc-TiO_2/dye2/P3HT thin films.

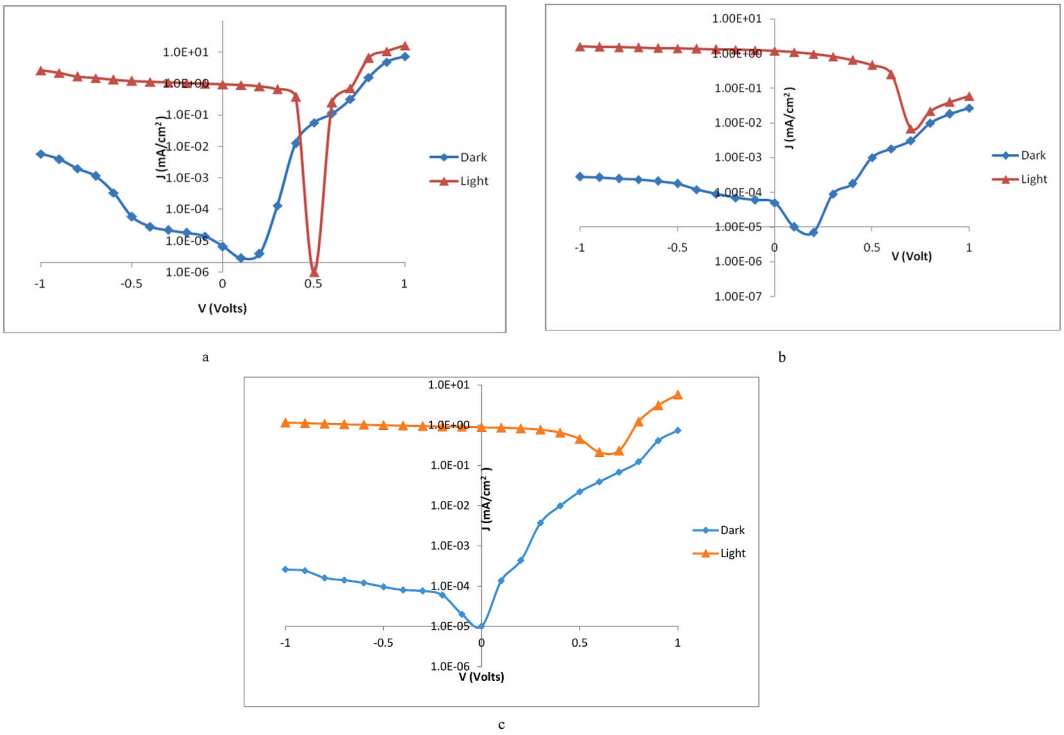

Fig. 4. aLog J-V characteristics of a P3HT/nc-TiO_2 solar cells
bLog J-V characteristics of a P3HT/dye1/nc-TiO_2 solar cells.
cLog J-V characteristics of a P3HT/dye2/nc-TiO_2 solar cells.

Edwards AUTO 306 turbo evaporation system. To provide illumination for the device, a xenon lamp was utilized. For measuring the current-voltage (I–V) characteristics, a Keithley 237 Source Measure Unit was employed.

The parameter of solar cells, fill factor FF, and power conversion efficiency μ, were determined using equations (1) and (2), where P_L is the power of imput light (100 mW/cm^2), Jsc is short circuit current density and V_{oc} is open circuit voltage.

$$FF = \frac{P_{\max}}{V_{oc} J_{Sc}} \tag{1}$$

$$\mu = \frac{P_{max}}{P_L} \tag{2}$$

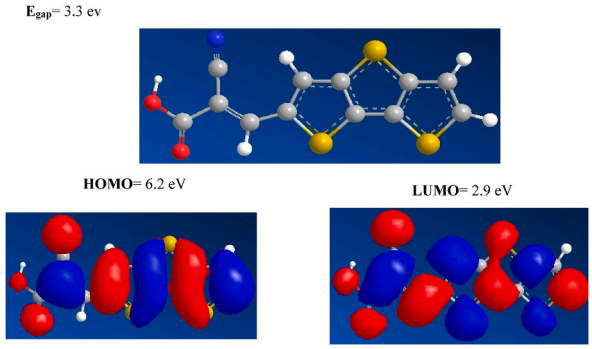

Fig. 5. Chemical Structure and molecular orbital of dye 1.

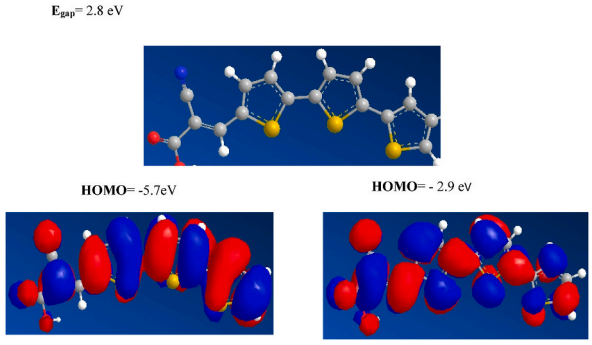

Fig. 6. Chemical Structure and molecular orbital of dye 2.

2.8. Results and discussion

The UV–visible absorption spectra of the nc-TiO_2/SnO_2:F, nc-TiO_2/P3HT, nc-TiO_2/dye 1/P3HT and nc-TiO_2/dye2/P3HT thin films used in the construction of the solar cells were represented in Fig. 3. As can be seen, the dye materials improved the light absorption of solar cells over the whole range from 400 to 540 nm while hole transport materials (P3HT) improved it from 650 to 380 nm.This is related to the difference of energy gaps of materials used in this device. For example, the peak absorption of nc-TiO_2 at 380 nm is corresponding to optical energy gap of 3.3ev, while the peak absorption of P3HT/nc-TiO_2 at 530 nm is corresponding to optical energy gap (2.3ev) of P3HT layer.

Additionally, the added dye 1 and dye 2 layer between P3HT and nc-TiO_2, increases the absorption peak value for P3HT and nc-TiO2 and shifts to lower wavelength from 530 to 430 nm. Dye 2 absorbance was higher than the absorbance of dye 1 attributed to the resemblance in rings in chemical structure of P3HT and dye 2 and the increase in the number of P3HT chains packed in the solar cell active layer, which subsequently improve the absorption. Contrary, to Dye1 which shows less absorbance because its thiophene rings are rigid and affect the P3HT chains packing. The band gap in dye 2 is around 2.8ev and leads to improve absorption peak value in dye2 solar cells compared to dye 1 solar cells. However, the absorption was better in dye2 solar cells, the charge separation in dye 1 solar cells was higher for having a high energy gap of 3.2ev. Thus the total efficiency of dye1 solar cells was 0.3 % while dye 2 solar cells was 0.2 %. The rigidity of thiophene rings with P3HT structure had a positive effect on the performance of P3HT/nc-TiO2 solar cells. In simpler terms, when more rings were fused together in the thiophene building blocks, it will reduce the shunt resistance and improved the charge transport through the junction.

Two solar cells were constructed using synthesized dye 1 and 2 by inserting these dyes individually between P3HT and nc-TiO_2. The effect of dye structure on solar cells performance was studied and compared with solar cell without dye. Generally, the dyes should possess certain photophysical and electrochemical properties to increase the efficiency of solar cells. The conduction band of nc-TiO_2 should be placed lower with respect to the lowest unoccupied molecular orbital (LUMO) of dyes while nc-TiO_2 valence band potential was located far from highest occupied molecular orbital (HOMO). For example, Dimitra Daphnomili reported that the number of pyridine rings at the meso positions affect the photovoltaic properties which lead to improving the efficiency of DSSC [23]. This improvement can be attributed to further enhancement in electron injection efficiency and charge collection efficiency. Here, under dark and light conduction, Fig. 4a–c shows the semi log plot of current versus voltage (J-V) characteristics of P3HT/nc-TiO_2, P3HT/dye1/nc-TiO_2 and P3HT/dye2/nc-TiO_2 solar cells respectively.

In the dark, the devices behave like a good diode with high rectification ratio estimated to be 103 $\pm$1 V for P3HT/nc-TiO_2 solar cell and P3HT/dye2/nc-TiO2 solar cell while, 100 at $\pm$1 V for P3HT/dye1/nc-TiO_2 solar cell. Additionally, the dye 1 solar cell showed

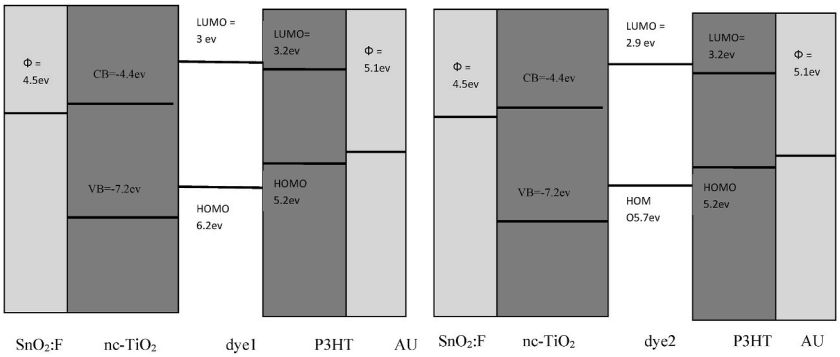

Fig. 7. Illustration of the energy level diagram for P3HT/dye/nc-TiO_2 solar cells.

lowest dark current compared to other cells when the device was under forward and reverse bias conditions. This is because of the difference in properties of interfacial layers of solar cells which depends on energy level alignment between hole transport material, dye materials and electron transport materials and/or with the work function of the bottom and the top electrodes. The dye 2 solar cell showed resemblance in the rectification ratio with P3HT/nc-TiO_2 because the chemical structure of dye 2 is almost same as P3HT. The only difference in dark curves comes from the increase in the shunt resistance which causes to reduce the dark current in P3HT/dye2/nc-TiO_2 under reverse bias condition in comparison with P3HT/nc-TiO2 solar cells. On the other hand, the energy levels of dye 1, which has rigid rings that may alter the energy level alignment at the P3HT/nc-TiO2 interface, result in lower dark current and a low rectification ratio. This phenomenon has been confirmed through Density Functional Theory (DFT) calculations [18–21,24]. The calculations employed the B3LYP functional, a three-parameter compound functional developed by Becke, along with a 6-31G(d) basis set to optimize the highest occupied molecular orbital (HOMO) and lowest unoccupied molecular orbital (LUMO) energies for the dyes. The molecular orbital (MO) surfaces visually depict the different stable electron distributions within a molecule.

According to Frontier Orbital theory, the shapes and symmetries of the HOMO and LUMO play a crucial role in predicting a species' reactivity and the stereochemical and regiochemical outcomes of chemical reactions. Figs. 5 and 6 illustrate the HOMO and LUMO of dye 1 and dye 2 compounds, respectively. The energy gap between the highest occupied and lowest unoccupied molecular orbitals, known as the frontier molecular orbital gap, provides insights into the molecule's chemical reactivity and kinetic stability. In the figures, the red color represents a positive charge, while the blue color represents a negative charge for the respective molecules. The HOMO acts as an electron donor, while the LUMO serves as an electron acceptor. The calculated energy values for dye 1 are −6.166 eV for the HOMO and −2.994 eV for the LUMO, whereas for dye 2, the values are −5.739 eV for the HOMO and −2.981 eV for the LUMO.

The calculated HOMO and LUMO energies clearly indicate the occurrence of charge transfer within the molecules. Moreover, the calculated HOMO-LUMO energy gap values are 3.3 eV for dye 1 and 2.8 eV for dye 2.

$\mathbf{E_{gap}} = 3.3$ ev

$\mathbf{E_{gap}} = 2.8$ eV

To explain the differences in efficiency of solar cells produced from the prepared dyes, P3HT and nc-TiO_2, the energy levels diagram of these materials are investigated. Such a diagram is presented in Fig. 7 based on literature values and our calculations. Relative to the vacuum level, the conduction and valence bands of the nc-TiO_2 are believed to lie at ~ -4eV and −7.2eV respectively, giving an energy gap of 3.2eV which is close to that determined by our STS [25]. The HOMO and LUMO levels for P3HT are at −3.2eV and −5.2eV respectively, yielding an optical gap of 2eV, which is again consistent with the optical absorption edge of P3HT seen in Fig. 3. The HOMO and LUMO levels of the dyes depend on their molecular electronic structure. The HOMO of the two dyes is intermediate between the LUMO of P3HT and the nc-TiO2 conduction band while the LUMO of the two dyes has the same value which is equal to 3 ev. On other hand, the HOMO of dye 1 is lower than the HOMO of dye 2 by 0.5ev. The high work function of gold/cathode, ~5.1eV, ensures a good Ohmic contact for holes from the P3HT, while the lower work function of the SnO_2:F contact/Anode (4.5eV) ensures facile electron transport to and from the bottom contact. The energy gap between the highest occupied molecular orbital (HOMO) and the lowest unoccupied molecular orbital (LUMO) plays a crucial role in determining the separation energy of exciton pairs in a material. The driving separation force results from the difference between the LUMO and HOMO and LUMO of dyes and hole and electron transport materials. The steps of energy levels in dye 1 with P3HT and nc-TiO2 was larger than in dye 2 with P3HT and nc-TiO2, which affect the conversion of light falling on the device to photo current. The flow of electrons and holes across the junction depends on the differences between the work function of electrodes and HOMO and LUMO of active layer in solar cells, the work function is essential for both electron and hole transfer processes in different materials and electronic devices, It determines the energy required for electron emission or hole injection/extraction, and it plays a pivotal role in shaping the electronic behavior and performance of semiconductor devices.

It is already known that charge extraction and transport in organic/dye/metal oxide solar cells are strongly influenced by the interfaces, in particular, the energy level alignment (ELA) [13,26]. Here, the difference in parameters of three solar cells is attributed to the energy levels alignment at interfaces between P3HT and nc-TiO_2 with dyes. The energy level of dye 1 allows easily hopping charges

Table 1
Photovoltaic parameters of solar cells with dyes 1 and 2 and without dye.

Parameters	P3HT/nc-TiO_2 Solar cells	P3HT/dye1/nc-TiO_2 Solar cells	P3HT/dye2/nc-TiO_2 Solar cells
Jsc(mA/cm^2)	0.9	1.2	0.88
Voc	0.5	0.7	0.625
μ %	0.2	0.3	0.2
FF %	44	32	36

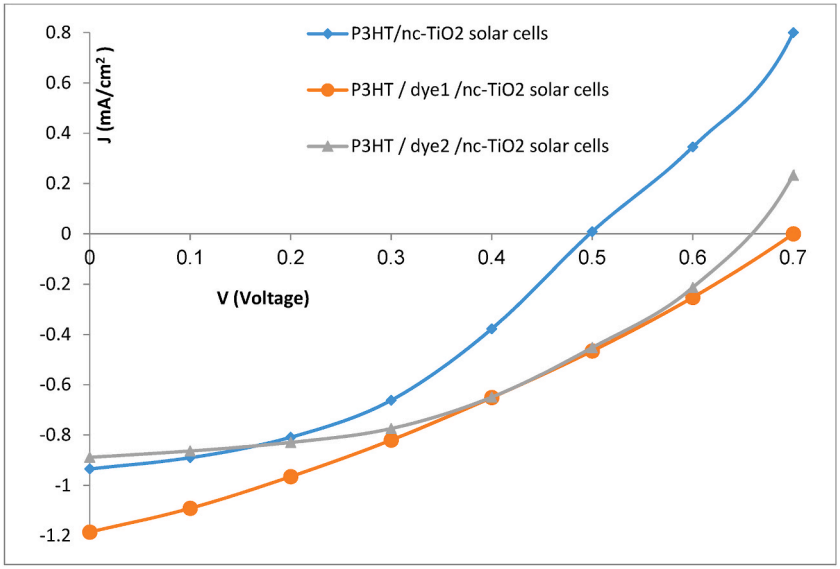

Fig. 8. J-V characteristics of the nc-TiO_2/dye 1/P3HT, nc-TiO_2/dye 2/P3HT and nc-TiO_2 /P3HT solar cells under light illumination.

through the interface. This is confirmed by determining the position of HOMO of dye 1 between the HOMO of P3HT and the nc-TiO_2 valence band. That may improve the charge separation at the interface because there is a step of 1 V between the HOMO of dye1 and valence band of nc-TiO_2 and HOMO of P3HT. The aforementioned argument aligns with existing literature findings, which highlight the importance of achieving the highest driving force for dye regeneration. It is crucial to finely tune the energy alignment between the lowest unoccupied molecular orbital (LUMO) of the dye and the conduction band of the semiconductor to ensure efficient electron injection. Additionally, the highest occupied molecular orbital (HOMO) of the dye should be positioned significantly lower than the energy level of the hole transport layer for successful dye regeneration. Table 1 provides a summary of the photovoltaic parameters for three solar cells fabricated under light illumination, which are extracted from J-V curves as shown in Fig. 8.

3. Conclusion

A lot of researches have been conducted to produce new dye materials for metal oxide/organic solar cells. The influence of dyes structure based on the π-conjugated rigidity of the thiophene rings on the photovoltaic characteristics has been investigated. The structure of the dye 1 prepared as sensitizers based on dithieno[3,2-*b*:2′,3′-*d*] thiophene-2-cyanoacrylic acid had the highest power conversion efficiency and short current density compared with the dye 2 which is based on [2,2':5′,2″-terthiophene]-5-cyanoacrylic. The HOMO of dye 1 is located at the middle between the VB of nc-TiO2 and HOMO P3HT while the HOMO of dye 2 is close to HOMO of P3HT. These differences explain the highest efficiency of dye 1 solar cells which results in improving the charge separation at the interface.

CRediT authorship contribution statement

Samir Al-Taweel: Writing – original draft, Methodology, Formal analysis. **Salah Al-Trawneh:** Writing – original draft, Methodology. **Hmoud Al-Dmour:** Writing – original draft, Methodology. **Osamah Al-Gzawat:** Al-Gzawat, Methodology, Investigation. **Wasim Alhalasah:** Software. **Marwan Mousa:** Mousa2, Resources, Formal analysis.

Declaration of competing interest

The authors declare that they have no known competing financial interests or personal relationships that could have appeared to influence the work reported in this paper.

Acknowledgements

The authors woud like to thank Scientific Research and Innovation Support Fund, Ministry of Higher Education and Scientific Research, Jordan, Amman, for their financial support.

References

[1] M. Kokkonen, P.-10 Talebi, J. Zhou, S. Asgari, S. Soomro, F. Elsehrawy, J. Halme, S. Ahmad, A. Hagfeldt, S. Hashmi, Advanced research trends in dye-sensitized solar cells, J. Mater. Chem. A 9 (17) (2021), 10527545, https://doi.org/10.1039/D1TA00690H.

[2] a) J. Baxter, Commercialization of dye-sensitized solar cells: present status and future research needs to improve efficiency , stability, and manufacturing, J. Vac. Sci. Technol. A 30 (2) (2012), 020801-020801-19, https://doi:10.1116/1.3676433;
b) S. Zhang, F. Huang, X. Guo, Y. Xiong, Y. Huang, H. Ågren, L. Wang, J. Zhang, Boosting the efficiency of dye-sensitized solar cells by a multifunctional composite photoanode to 14.13 %, Angew. Chem. 135 (23) (2023), e202302753 https://doi.org/10.1002/anie.202302753;
c) L. Mao, S. Dun, H. Ren, J. Jiang, X. Guo, F. Huang, P. Heng, L. Wang, J. Zhang, H. Agren, Introducing chenodeoxycholic acid coadsorbent and strong electron-withdrawing group in indoline dyes to design high-performance solar cells: a remarkable theoretical improvement, J. Mater. Chem. C 9 (17) (2021) 5800–5807, https://doi.org/10.1039/D0TC05665K.

[3] B. O'Regan, M. Grätzel, A low-cost, high-efficiency solar cell based on dye-sensitized colloidal TiO_2 films, Nature 353 (2) (1991) 737–740, https://doi.org/10.1038/353737a0.

[4] H. Al-Dmour, R. Alzard, H. Alblooshi, K. Alhosani, S. AlMadhoob, N. Saleh, Enhanced energy conversion of Z907-based solar cells by Cucurbit [7] uril macrocycles, Front. Chem. 7 (2019) 561, https://doi.org/10.3389/fchem.2019.00561.

[5] A. Mishra, M. Fischer, M, P. Bäuerle, Metal-free organic dyes for dye-sensitized solar cells: from structure: property relationships to design rules, Angew. Chem. Int. Ed. 48 (14) (2009) 2474–2499, https://doi.org/10.1002/anie.200804709.

[6] A. Yella, H. Lee, H. Tsao, K. Chandiran, K. Nazeeruddin, G. Diau, Y. Yeh, M. Zakeeruddin, M. Gratzel, Porphyrin-sensitized solar cells with cobalt (II/III)-based redox electrolyte exceed 12 percent efficiency, 334, Science 4 (6056) (2011) 629–634, https://DOI:10.1126/science.1209688.

[7] M. Nazeeruddin, I. Rodicio, H. Baker, E. Mueller, N. Liska, N. Vlachopoulos, M. Grätzel, Conversion of light to electricity by cis-X2bis(2,2'-bipyridyl-4,4'-dicarboxylate)ruthenium(II) charge-transfer sensitizers (X = Cl-, Br-, I-, CN-, and SCN-) on nanocrystalline titanium dioxide electrodes, J. Am. Chem. Soc. 115 (14) (1993) 6382–6390, https://doi.org/10.1021/ja00067a063.

[8] A. Hagfeldt, G. Boschloo, L. Sun, L. Kloo, H. Pettersson, Dye-sensitized solar cells, Chem. Rev. 110 (11) (2010) 6595–6663, https://doi.org/10.1021/cr900356p.

[9] K. Sharma, V. Sharma, S. Sharma, Dye-sensitized solar cells: fundamentals and current status, Nanoscale Res. Lett. 13 (2018) 381, https://doi.org/10.1186/s11671-018-2760-6.

[10] L. Calió L, S. Kazim, M. Grätzel, S. Ahmad, Hole-transport materials for perovskite solar cells, 47, Angew Chem. Int. Ed. Engl. 14 (55) (2016) 14522–14545, https://doi.org/10.1002/anie.201601757.

[11] P. Vivo, J.K. Salunke, A. Priimagi, Hole-transporting materials for printable perovskite solar, Materials 10 (9) (2017) 1087, https://doi.org/10.3390/ma10091087.

[12] a) H. Qin, S. Wenger, M. Xu, F. Gao, X. Jing, P. Wang, S. Zakeeruddin, M. Gratzel, An organic sensitizer with a fused dithienothiophene unit for efficient and stable dye-sensitized solar cells, J. Am. Chem. Soc. 130 (29) (2008) 9202–9203, https://doi.org/10.1021/ja8024438;
b) M. Hend, A. Abdel-Wahed, F. Abdel-Latif, S. Abdelmageed, M. Elmorsy, Novel triphenylamine-based porphyrins: synthesis, structural characterization, and theoretical investigation for dye-sensitized solar cell applications, J. Mol. Struct. 1281 (2023), 135147, https://doi.org/10.1016/j.molstruc.2023.135147;
c) M. Elmorsy, S. Badawy, K. Salem, A. Fadda, E. Abdel-Latif, New photosensitizers that are based on carbazoles and have thiophene bridges with a low bandgap do 32% better than N719 metal complex dye, J. Photochem. Photobiol. A :Chem. 436 (2023), 114421, https://doi.org/10.1016/j.jphotochem.2022.114421.

[13] N. Saleh, S. Al-Trawneh, H. Al-Dmour, S. Al-Taweel, J. Graham, Effect of molecular-level insulation on the performance of a dye-sensitized solar cell: fluorescence studies in solid state, J. Fluoresc. 25 (1) (2015) 59–68, https://doi.org/10.1007/s10895-014-1479-8.

[14] T. Kodama, I. Nakajima, M. Kumada, Nickel-phosphine complex-catalyzed Grignard coupling - II: grignard coupling of heterocyclic compounds, Tetrahedron 38 (22) (1982) 3347–3354, https://doi.org/10.1016/0040-4020(82)80117-8.

[15] H. Al-Dmour, S. Al-Trawneh, S. Al-Taweel, Synthesis, characterization, and performance of oligothiophenecyanoacrylic acid derivatives for solar cell applications, Int. J. Adv. Appl. Sci. 8 (6) (2021) 128–135, https://doi.org/10.21833/ijaas.2021.06.015.

[16] F. Joseph, S. Proemmel, M. Armitage, B. Holmes, Synthesis of dithieno[3,2-b:2',3'-d]thiophene, Org. Synth. 83 (2006) 209, https://doi.org/10.15227/orgsyn.083.0209.

[17] A. Vilsmeier, A. Haack, The effect of halogen phosphor on alkyl formanilide - a new method for the characterization of secondary and tertiary p-alkyl amino-benzaldehyde, Chem. Ber. 60 (1927) 119–122, https://doi.org/10.1002/cber.19270600118.

[18] P. Hohenberg, W. Kohn, Inhomogeneous electron gas, Phys. Rev. 136 (1964) B864, https://doi.org/10.1103/PhysRev.136.B864.

[19] W. Kohn, L. Sham, Self-consistent equations including exchange and correlation effects, 1965, Phys. Rev. 140 (1965) A1133, https://doi.org/10.1103/PhysRev.140.A1133.

[20] D. Salahub, M. Zerner (Eds.), The Challenge of D and F Electrons, ACS, Washington, DC, 1990, https://doi.org/10.1002/crat.2170250603.

[21] R. Parr, W. Yang, Density-functional Theory of Atoms and Molecules, Oxford University Press, Oxford, 1989, https://doi.org/10.1002/qua.560470107.

[22] H. Al-Dmour, D. Taylor, J. Cambridge, Effect of nanocrystalline-TiO2 morphology on the performance of polymer heterojunction solar cells, J. Phys. Appl. Phys. 40 (2007) 5034, https://doi.org/10.1088/0022-3727/40/17/004.

[23] D. Daphnomili, G. Landrou, S. Singh, A. Thomas, K. Yesudas, B. hanuprakash G. Sharma, A. Coutsolelos, Photophysical, electrochemical and photovoltaic properties of dye sensitized solar cells using a series of pyridyl functionalized porphyrin dyes, RSC Publ. RSC Adv. 2 (33) (2012) 12899–12908, https://doi.org/10.1039/C2RA22129B.

[24] M.J. Frisch, G.W. Trucks, H.B. Schlegel, G.E. Scuseria, M.A. Robb, J.R. Cheeseman, G. Scalmani, V. Barone, G.A. Petersson, H. Nakatsuji, X. Li, M. Caricato, A. Marenich, J. Bloino, B.G. Janesko, R. Gomperts, B. Mennucci, H.P. Hratchian, J.V. Ortiz, A.F. Izmaylov, J.L. Sonnenberg, D. Williams-Young, F. Ding, F. Lipparini, F. Egidi, J. Goings, B. Peng, A. Petrone, T. Henderson, D. Ranasinghe, V.G. Zakrzewski, J. Gao, N. Rega, G. Zheng, W. Liang, M. Hada, M. Ehara, K. Toyota, R. Fukuda, J. Hasegawa, M. Ishida, T. Nakajima, Y. Honda, O. Kitao, H. Nakai, T. Vreven, K. Throssell, J.A. Montgomery Jr., J.E. Peralta, F. Ogliaro, M. Bearpark, J.J. Heyd, E. Brothers, K.N. Kudin, V.N. Staroverov, T. Keith, R. Kobayashi, J. Normand, K. Raghavachari, A. Rendell, J.C. Burant, S.S. Iyengar,

J. Tomasi, M. Cossi, J.M. Millam, M. Klene, C. Adamo, R. Cammi, J.W. Ochterski, R.L. Martin, K. Morokuma, O. Farkas, J.B. Foresman, D.J. Fox, Gaussian 09, Revision A.02, Gaussian, Inc., Wallingford CT, 2016.

[25] H. Al Dmour, Utilizing spectroscopy and optical microscopy to characterize titanium dioxide thin films, East Eur. J. Phys. 4 (2022) (2022) 171–175, https://doi.org/10.26565/2312-4334-2022-4-17.

[26] J. Pei, Y.Z. Hao, H.J. Lv, et al., Optimizing the performance of TiO2/P3HT hybrid solar cell by effective interfacial modification, Chem. Phys. Lett. 644 (2016) 127–131, https://doi.org/10.1016/j.cplett.2015.11.058.